Am J Physiol Cell Physiol 282: C1076–C1086, 2002.
First published December 12, 2001; 10.1152/ajpcell.00210.2001.

Excess plasma membrane and effects of ionic amphipaths on mechanics of outer hair cell lateral wall

NORIKO MORIMOTO, ROBERT M. RAPHAEL,
ANDERS NYGREN, AND WILLIAM E. BROWNELL
Department of Otorhinolaryngology and Communicative Science, Baylor College of Medicine, Houston, Texas 77030

Received 7 May 2001; accepted in final form 10 December 2001

Morimoto, Noriko, Robert M. Raphael, Anders Nygren, and William E. Brownell. Excess plasma membrane and effects of ionic amphipaths on mechanics of outer hair cell lateral wall. *Am J Physiol Cell Physiol* 282: C1076–C1086, 2002. First published December 12, 2001; 10.1152/ajpcell.00210.2001.—The interaction between the outer hair cell (OHC) lateral wall plasma membrane and the underlying cortical lattice was examined by a morphometric analysis of cell images during cell deformation. Vesiculation of the plasma membrane was produced by micropipette aspiration in control cells and cells exposed to ionic amphipaths that alter membrane mechanics. An increase of total cell and vesicle surface area suggests that the plasma membrane possesses a membrane reservoir. Chlorpromazine (CPZ) decreased the pressure required for vesiculation, whereas salicylate (Sal) had no effect. The time required for vesiculation was decreased by CPZ, indicating that CPZ decreases the energy barrier required for vesiculation. An increase in total volume is observed during micropipette aspiration. A deformation-induced increase in hydraulic conductivity is also seen in response to micropipette-applied fluid jet deformation of the lateral wall. Application of CPZ and/or Sal decreased this strain-induced hydraulic conductivity. The impact of ionic amphipaths on OHC plasma membrane and lateral wall mechanics may contribute to their effects on OHC electromotility and hearing.

membrane reservoir; electromotility; membrane bending; hearing; hydraulic conductivity

THE OUTER HAIR CELL (OHC) contributes to fine-tuning in the mammalian inner ear through its unique membrane potential-dependent motility. OHC electromotility is a shape change that results from the direct conversion of electrical potential into a mechanical force (6). It does not depend on calcium or intracellular stores of ATP (7, 30). The mechanism underlying electromotility is associated with the plasma membrane and its lipid environment. This membrane motor transmits force via the OHC cytoskeleton to produce cell deformation. Cellular micro- and nanomechanics are integral to the mechanism of OHC force production (9). Theoretical models predict that passive mechanical properties of the OHC should affect electromotility (29, 52, 72, 73). The protein prestin was recently isolated and demonstrated to be involved in the motor mechanism (36, 63, 78) along with small anions (44). These findings provide support for the hypothesis that electromotility is associated with the conformational change of an integral membrane protein (13, 29, 62). Hence, the mechanical properties of the plasma membrane (PM) should influence the function of the protein and therefore electromotility. Although the motor is often specified to be an area motor, any out-of-plane bending of the membrane (as commonly occurs in biological membranes) would greatly decrease the efficiency of such a mechanism. Ionic amphipaths readily insert into membranes and are known to alter the curvature and mechanics of erythrocytes (66) as well as OHC mechanics (15, 24, 32, 37, 46, 59, 67, 74, 77). These molecules may be used to probe the effects of membrane curvature on OHC function.

The OHC lateral wall is a trilaminate structure composed of the PM, cortical lattice (CL), and subsurface cisterna (SSC). Electron micrographs reveal that the outermost layer PM is rippled (15, 70) whereas the membrane of the outermost layer of the SSC presents a flat, crisp bilayer appearance (15, 60). The CL, sandwiched between the SSC and the PM, is arranged in cytoskeletal microdomains of parallel actin filaments cross-linked with spectrin (21, 25–27). Bridging the distance between the actin filaments and the PM are structures of unknown composition called pillars (2, 3, 21). The OHC is a cellular hydrostat with a positive turgor pressure. This pressure maintains the cell shape and is required for the full expression of the electromotile response (5, 31, 61, 67). The regulation of cell volume and cytoplasmic pressure is particularly important for the OHC, and previous studies explored the effective water permeability of the OHC PM (8, 11, 56).

Micropipette aspiration is a technique that measures cell mechanical properties and has been applied to lipid vesicles and red blood cells (4, 18). This technique has also been applied to the OHC to measure the "stiffness

Address for reprint requests and other correspondence: W. E. Brownell, Dept. of Otorhinolaryngology and Communicative Sci., NA 505, Baylor College of Medicine, Houston TX 77030 (E-mail: brownell@bcm.tmc.edu; http://www.bcm.tmc.edu/oto/research/cochlea/index.html).

The costs of publication of this article were defrayed in part by the payment of page charges. The article must therefore be hereby marked "*advertisement*" in accordance with 18 U.S.C. Section 1734 solely to indicate this fact.

parameter" of the lateral wall (37, 42, 69). Because of the orthotropic nature of the cell, this stiffness parameter is a combination of its axial and radial stiffness (71), both of which have components originating from the membrane and cytoskeleton. These experiments revealed that as the pressure was increased, vesiculation of the PM occurred (69). Oghalai et al. (42), using fluorescence labeling specific for the PM, F-actin, and SSC, showed that the vesicles contained only the PM label. In the study reported here, we used the micropipette aspiration technique and morphometrically analyzed the vesiculation process. The results demonstrate the existence of excess PM in the OHC. The existence of membrane reservoirs in fibroblasts has been demonstrated with tether formation experiments, in which narrow membranous tubes are pulled from the surface of a cell (57). We have applied this technique and demonstrated excess membrane in OHCs (1, 35). A membrane reservoir is important in the function of endothelial cells and neutrophils (64). Membrane unfolding is also believed to play a role in other cells, such as the response of alveolar epithelial cells to mechanical forces in the lung (76).

We also investigated the effect of altering membrane mechanics with ionic amphipaths. The anionic amphipath salicylate (Sal) diminishes OHC electromotility (67), decreases OHC axial stiffness, and decreases OHC force production (24). The lateral wall stiffness parameter is also affected by Sal (37). In this report, we extend previous studies of the effect of Sal on membrane mechanics by exploring how Sal affects the vesiculation process. In addition, we investigated the effect of the cationic amphipath chlorpromazine (CPZ), because of its effects on the red blood cell as well as our observation that it alters lipid lateral diffusion in the PM of the OHC (43) and translates the voltage-displacement function for OHC electromotility toward depolarizing potentials (38). Both drugs reduced the aspiration-associated increase in water permeability observed in OHCs. The findings presented here indicate that Sal and CPZ change the mechanical properties of OHC membranes consistent with their effects on OHC electromotility and hearing. A preliminary version of these results was presented previously (40).

MATERIALS AND METHODS

OHC isolation. Albino guinea pigs weighing 200–400 g were decapitated by guillotine. The temporal bones were taken, and the middle ear bullae were opened. The otic capsule was removed, and the spiral ligament was peeled off to expose the organ of Corti. The organ of Corti was dislodged from the cochlea and harvested in a standard medium. OHCs were isolated from the organ of Corti by gentle trituration without enzyme (11). All OHCs were plated onto a glass coverslip cemented to the bottom of a plastic chamber. Isolated cells were selected for study on the basis of standard morphological criteria within 3 h of animal death. Healthy cells displayed a characteristic birefringence and a transparent cytoplasm, the nucleus was in the base of the cell, and cells possessed a uniformly cylindrical shape without regional swelling. Cells were excluded if Brownian motion of intracellular particles was observed.

Solutions. The standard medium was composed of HEPES-buffered extracellular solution supplemented with (in mM) 135 NaCl, 4 KCl, 1 $MgCl_2$, 2 $CaCl_2$, 10 HEPES, and 10 glucose. The solution had an osmolarity of 285–290 mosM and a pH of 7.4 and was at room temperature (22–24°C). The hypotonic solution consisting of the standard medium and distilled water was adjusted to an osmolarity of 250 mosM and a pH of 7.4.

For some experiments, 10 mM sodium salicylate (S-3007, Sigma, St. Louis, MO) and/or 0.1 mM CPZ (C-8138, Sigma) were added to the extracellular solution. Each drug was dissolved in the extracellular solution at twice the desired concentration. A volume of the 2× drug solution was added to an equal volume of the control solution containing OHCs. Each experiment was started within 10 min of application of drugs and was finished in 40 min.

Experimental protocols and data collection. A chamber containing cells was placed onto the stage of an inverted microscope (Zeiss Axiovert 135TV), and the cells were imaged using an oil-immersion ×100 objective lens. A Dage MTI Newvicon video camera was used to capture images. Either negative or positive pressure applied via a small-diameter pipette was used to deform the OHC lateral wall. A negative pressure was applied during micropipette aspiration. A positive pressure was applied to a pipette containing hypoosmotic extracellular medium (250 mosM) to produce a fluid jet. Both protocols were followed after application of 10 mM Sal, 0.1 mM CPZ, or both. The response of the OHC was monitored on a television screen and recorded with a videocassette recorder (Panasonic AG1960, S-VHS). The time and date were superimposed and recorded on the video image. The level of the water column and other experimental details were recorded on one of the audio channels.

Micropipette aspiration. Aspiration micropipettes were fabricated from borosilicate glass capillary (LG16, 1.65-mm OD, 1.1-mm ID; Dagan, Minneapolis, MN) with a programmable micropipette puller (BB-CH-PC; Mecanex, Geneva, Switzerland). The inner diameter of the tip was ~3 μm and was fire-polished with a microforge (Microforge De Fonbrune; Aloe Scientific, St Louis, MO).

The micropipette was connected to a water column via a polyethylene tube that was filled with the extracellular solution and 0.2 mg/ml bovine serum albumin (Sigma). The micropipette was mounted on a joystick-controlled manipulator (Zeiss) and advanced at a shallow angle (<20° against the stage) at the center of the field of view. The zero pressure point of the water column was referenced to the level of the microscope stage and was defined as the water level at which no flow in or out of the micropipette was observed.

Once a cell was located, the micropipette was brought into contact with the side of the OHC midway on its lateral wall. Negative pressure was applied in a stepwise manner as measured from the null point until vesiculation occurred. Initially, the entire trilaminate lateral wall is aspirated into the pipette. Eventually, the PM separates from the underlying CL and only the PM continues to elongate. The PM pinches off and forms a vesicle that is composed solely of PM (42). Several vesicles were removed from each cell by aspiration. The maximum number of vesicles that can be removed varies from cell to cell. More than 20 vesicles have been removed from long OHCs (69). When a cell-specific number of vesicles have been removed (presumably when all the excess PM has been exhausted), the membrane in the micropipette ruptures and there is a precipitous loss of cell volume as indicated by the collapse of the cell. At this point, the cell is often sucked into the micropipette and lost.

Morphometric analysis. A cell was subjected to morphometric analysis before and after vesicles were pulled. Analysis was made only if there was no Brownian motion of internal organelles. Single frames from the S-VHS tape were selected and digitized with NIH Image. Each image was traced five times per cell with a MATLAB program (Mathworks). The program was similar to an earlier morphometric analysis program (11). The surface area and volume of the cell are approximated as a sum of cylindrical segments, each with surface area

$$S_i = \Delta x \cdot 2\pi r_i \quad (1)$$

and volume

$$V_i = \Delta x \cdot \pi r_i^2 \quad (2)$$

Where Δx and r_i are the height and radius, respectively, of segment i. The whole cell was traced before aspiration. Each vesicle that pinched off during the aspiration process was traced. The cell was traced again after release of three, six, and nine vesicles. The resolution of the digitized images was 5.5 pixels/μm. The surface area and volume, length, and radius of the cell (defined as the average radius for segments in the middle 2/3 of the length of the cell) were calculated assuming radial symmetry about the long axis (Fig. 1*A*). The surface area and volume of the vesicle were calculated by dividing the vesicle into three sections. The center part was modeled as a cylinder, and both ends were modeled as hemispheres (Fig. 1*B*). An error analysis (see APPENDIX A) supports the conclusions based on these measurements.

Micropipette fluid jet protocol. Micropipettes with an inner diameter of ~5 μm were fabricated in the same manner as aspiration micropipettes. The micropipette was connected to a water column, and the entire fluid system was filled with hypotonic extracellular solution. Once a cell was located, the tip of the pipette was brought within 10 μm of the cell. The water column was raised up to +20 cmH_2O, and a jet of water on one side of the OHC was produced. A jet of hypoosmotic medium (250 mosM) produces a local dimpling of the lateral wall, and then the cell starts swelling. The associated volume increase as a function of time was analyzed to determine the local hydraulic conductivity (8, 56).

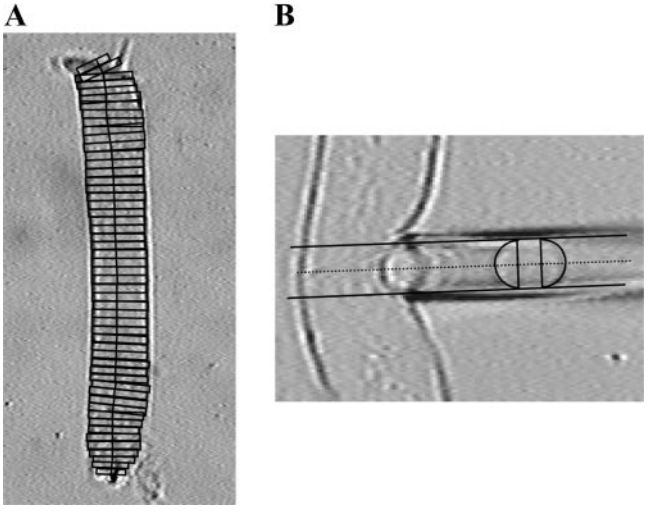

Fig. 1. Morphometric analysis of the outer hair cell (OHC) and vesicle. *A*: segmentation of an OHC image. The surface area and volume, length, and radius of the cell were calculated assuming radial symmetry about the long axis. *B*: vesicle analysis. The surface area and volume of the vesicle were calculated by dividing the vesicle into 3 sections. The center part was assumed to be a cylinder, and both ends of the cap were assumed to be a part of a sphere.

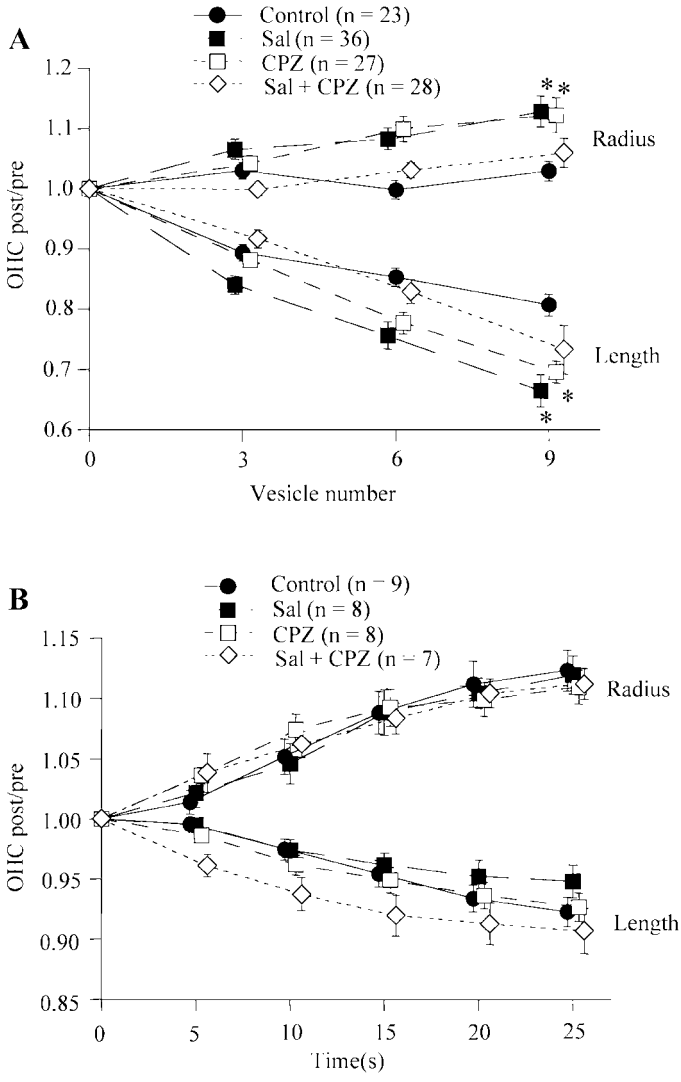

Fig. 2. Change of OHC length and radius. *A*: mean length and radius of cells after removal of 3, 6, and 9 vesicles during aspiration. *B*: mean length and radius of cells during fluid jet protocol. Values are means ± SE (*$P < 0.01$, repeated-measures ANOVA). Sal, salicylate; CPZ, chlorpromazine.

The whole cell was traced before application of the fluid jet. The cell was traced after 5, 10, 15, and 20 s and the length, radius, surface area, and volume were calculated with the MATLAB program described in *Morphometric analysis*.

RESULTS

Cell shape changes during micropipette aspiration. The effects of removing PM vesicles on the geometry of the OHC are summarized in Fig. 2*A*, which shows the length and the radius of the cell during aspiration. Control OHCs maintained a constant radius but decreased their length by 15% during the aspiration process. Exposure to either Sal or CPZ did not result in an immediate change in cell shape. However, these drugs did affect the behavior of the cell during the aspiration process. When either Sal or CPZ was ap-

plied, the length decrease was ~30% and the radius increase was ~10% more than that of control cells. When Sal and CPZ were applied together, the cell's shape change resembled that of control cells. Figure 2*B* shows the OHC length and radius change accompanied by cell swelling in response to the hypoosmotic fluid jet. A length decrease of ~5% and a radius increase of 10% were observed for all groups.

Surface area change. The total surface area for the OHC and the sum of the removed vesicles was compared with the surface area of the cell before the aspiration process was initiated. The total mean surface area gradually increased ~7% for all groups (Fig. 3*A*). Removed original surface area was compared with total vesicle surface area (Fig. 3*B*). In almost all cases, the ratios of removed surface area from the OHC over the formed vesicle surface area are <1. This ratio should be 1 if membrane area is conserved. The total removed vesicle surface area exceeds the original apparent surface area of the cell, indicating that the intact OHC PM possesses excess PM. This excess membrane is likely stretched during aspiration and covers the vesicle when vesiculation occurs. There are no apparent drug effects on the control surface area of the PM. To observe whether the drugs affected the size of the vesicles, the surface area of each vesicle was compared (Fig. 3*C*) and was positively correlated with the pipette diameter unrelated to drug application. The results of the hypoosmotic fluid jet experiment confirm that the apparent surface area remains constant despite volume change (Fig. 3*D*) as previously reported (8). There are also no detectable drug effects on the apparent surface area, as is the case with aspiration.

Drug-induced mechanical property changes. Figure 4*A* presents the pressure required to remove the first vesicle in the aspiration protocol. CPZ decreased this pressure, whereas Sal did not change it. Even less pressure was required when both Sal and CPZ were present. The mean time to form subsequent vesicles was also measured (Table 1). The mean time between vesicles was greatest for control and Sal-treated cells; CPZ and Sal + CPZ reduced the time >50%. Because there were no differences in size among the vesicles, it appears that CPZ facilitates vesicle formation by decreasing the work required for vesiculation.

The relevant mechanical property for describing these drug effects is the tension within the lateral wall. To interpret the data in this context, we converted the aspiration pressure to an effective tension (see APPENDIX B). The results in Fig. 4*B* demonstrate the effect of drugs on the calculated tension required to form a vesicle. Sal increased and CPZ decreased the effective tension required to form a vesicle.

Drug effects on hydraulic conductivity of PM. The total volume of the OHC and sum of the removed vesicles was compared with the volume of the cell before the aspiration process was initiated (Fig. 5*A*). Cytosol was lost during aspiration for all groups. The

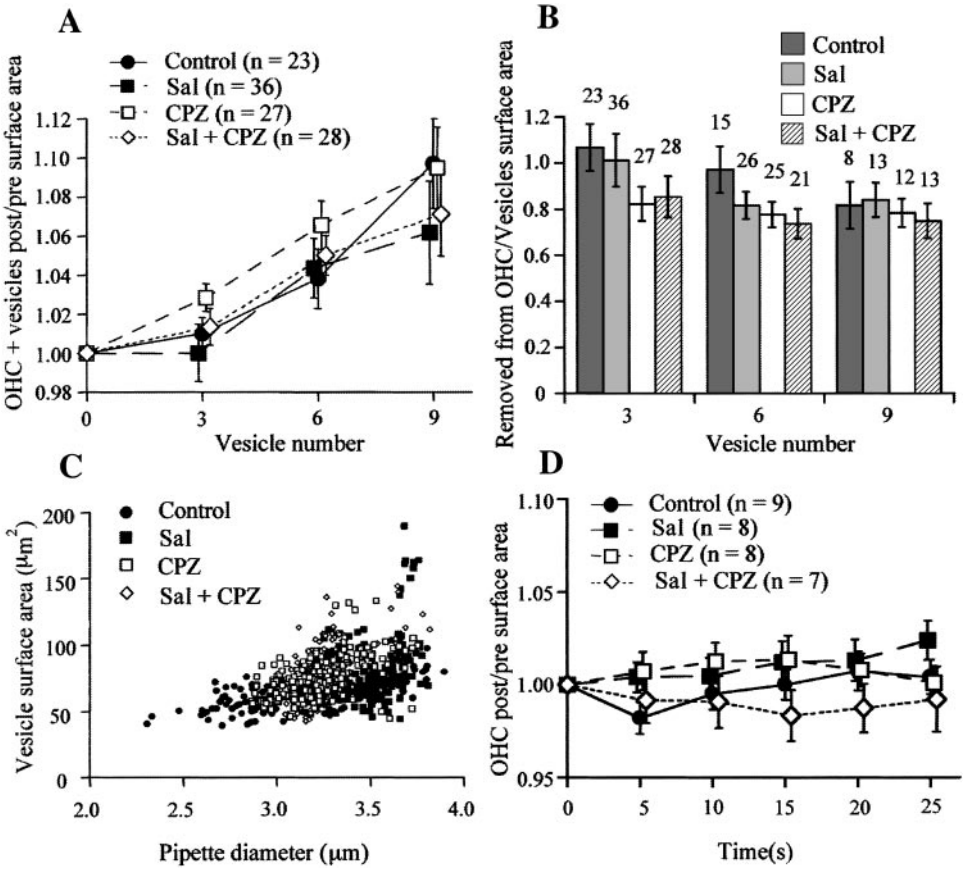

Fig. 3. Change of OHC surface area. *A*: total surface area increases for all groups during aspiration protocol. Values on the abscissa are the sum of the OHC surface area after aspiration of n (ordinate) vesicles plus the total area of the aspirated vesicles, divided by the OHC surface area before aspiration. Values are means ± SE. *B*: surface area removed from the original OHC surface area divided by total vesicle surface area. Vesicle surface area is larger than removed apparent surface area because these ratios are <1. The number above each bin in the histogram is n. Error bars indicate SE. *C*: surface area for each vesicle is proportional to the pipette diameter unrelated to the drug effects. *D*: surface area remains constant although the cell's volume increases dramatically during fluid jet protocol. Values are means ± SE.

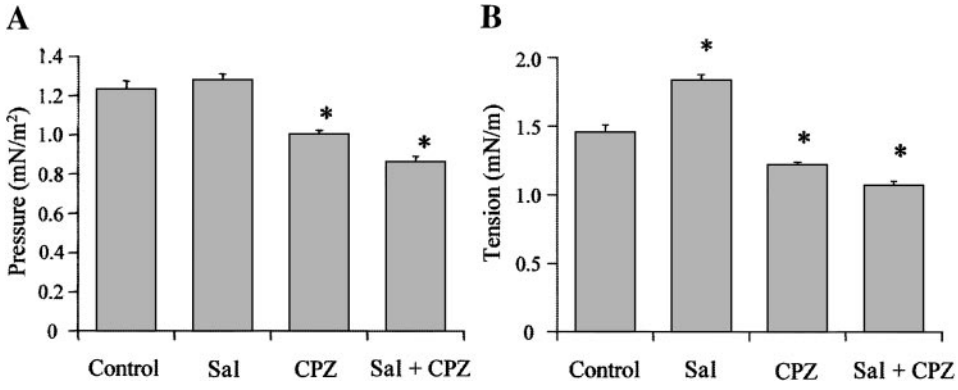

Fig. 4. *A*: pressure required to remove 1 vesicle. *B*: effective lateral wall tension to form the vesicle. The effective tension is calculated with *Eq. B3*. Error bars indicate SE (*$P < 0.001$, unpaired *t*-test). The same cells were used for both *A* and *B*. The number of cells was 134 control, 220 Sal, 192 CPZ, and 189 Sal + CPZ.

volume loss for control cells was ~13%, whereas CPZ-treated cells lost <5%. Figure 5*B* shows the proportion of cytosol leakage for each group. After six vesicles were removed, the amount of cytosol lost through leakage was half as large in Sal- and CPZ-treated cells as in control cells. There were no significant differences in the vesicle volume regardless of the drug applied. The strain-induced volume increase associated with perfusion with a hypoosmotic fluid jet was measured and plotted in Fig. 5*C*. The slope (L_p) of each plot is a measure of the hydraulic conductivity of the PM (8, 56). The plot for the control cells has a slope that is steeper than those for drug-treated cells.

DISCUSSION

The major observations of this study are that the OHC PM possesses excess membrane and that Sal and CPZ alter the cell's mechanical properties such as lateral wall tension and PM hydraulic conductivity. The excess surface area measured for nine vesicles (Fig. 3*A*) was slightly more than the excess represented by membrane folding as measured in an ultrastructural study on the OHC (75). Excess membrane or a membrane reservoir has also been observed while pulling membrane tethers from an OHC with optical tweezers (1, 35). The tether experiments reveal a strong attachment force between the membrane and the CL. After the membrane separates from the CL, the force required to pull a tether falls to a nearly constant value and tethers of >50 μm in length are routinely pulled. The force plateau demonstrates that no additional force is needed during this phase of tether elongation. If stretching of the membrane and/or underlying structures were involved, additional force would be required. Long membrane tethers that require no additional force for their formation are consistent with a membrane reservoir (57).

Table 1. *Pressure to first vesicle and mean time to form vesicles*

Drug	Pressure, (mN/m²)	*n*	*P* for *t*-Test	Time, s	*n*	*P* for *t*-Test
Control	1.26 ± 0.10	22		229.18 ± 21.6	22	
Sal	1.26 ± 0.07	36	0.998	254.57 ± 22.7	36	0.45
CPZ	0.96 ± 0.04	27	0.005	109.85 ± 16.2	27	<0.0001
Sal+CPZ	0.87 ± 0.05	28	0.0007	64.75 ± 11.0	28	<0.0001

Values are means ± SE for *n* cells. Sal, salicylate; CPZ, chlorpromazine.

The folded PM visible in transmission electron microscopy is an obvious source of excess membrane, but it is also possible that internal membranes contribute to the membrane reservoir. Micropipette aspiration experiments indicate that membrane insertion from internal stores does not occur before vesiculation. Micropipette aspiration studies on the kinetics of amphiphilic insertion reveal membrane insertion by a clearly visible increase in the projection length within the pipette at a constant aspiration pressure (41). In our experiments, the OHC projection length does not creep at constant pressure (42, 69), indicating that a deformation-induced membrane insertion does not occur before vesiculation. If membrane insertion did occur after vesiculation, the most likely source of internal membranes would be the SSC, and we demonstrated previously (42) that SSC membranes do not insert into PM during the formation of the first five or six vesicles. This finding is consistent with an earlier study showing that uptake of extracellularly applied horseradish peroxidase is not observed in the lumen of the SSC, indicating that the SSC belongs to a separate membrane pool than that of the endoplasmic reticulum-Golgi-PM (68). In addition, there has never been a report of vesicle fusion to the OHC PM for any location along the lateral wall where the intimate association between the CL and the PM might interfere with membrane fusion. There is evidence for membrane turnover at both the base and apex of the cell, where vesicle fusion has been shown ultrastructurally (68), and membrane recycling has been observed through imaging pinocytotic uptake of fluorescent-labeled PM (42). The insertion of additional membrane from internal membrane stores most likely occurs at these locations. The new membrane must then diffuse along the length of the lateral wall. For the fast, physiologically relevant changes in cell length and membrane tension associated with OHC function, an interaction with an internal membrane pool is probably not important. Hence, the most direct interpretation of our experiments is that after the attachment to the CL is broken, the overlying membrane is free to unfold and this is responsible for the experimentally observed excess

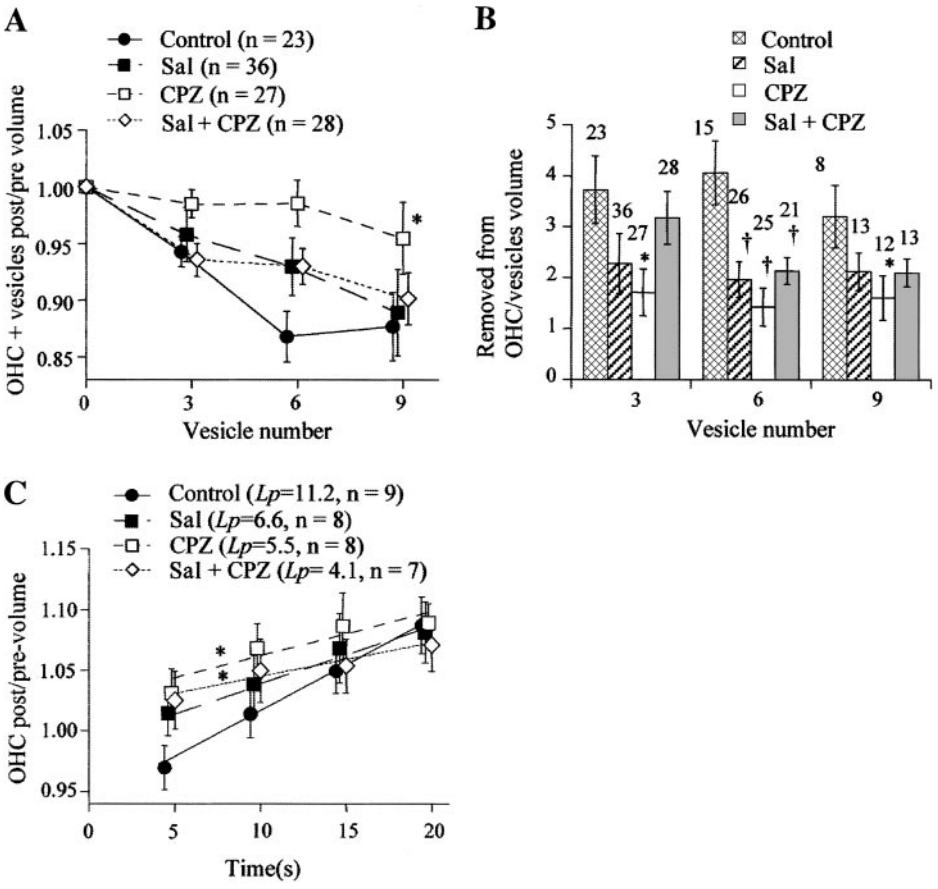

Fig. 5. *A*: total volume change throughout aspiration. Total pre- and postexperiment OHC and vesicle volume are compared. When CPZ was applied, volume was decreased less than those of control cells. Values are means ± SE (*$P < 0.05$, repeated-measures ANOVA). *B*: volume loss during aspiration. Removed original volume from OHC and vesicle volume is compared during aspiration. Removed original volume is more than twice greater than vesicle volume (*$P < 0.01$, †$P < 0.05$, unpaired *t*-test), which indicates cytosol leakage. Bars indicates SE. Top number of each histogram shows *n*. *C*: volume change during fluid jet. Volumes for OHC before and after hypoosmotic fluid jet protocol are compared. The slope (L_p; 10^{-14} $mPa^{-1}s^{-1}$) of each plot is a measure of the cell's hydraulic conductivity ($R > 0.9$). The slope for control cells is steeper than those of drug-treated cells. Values are means ± SE of 7–9 independent determination. CPZ- and Sal + CPZ-treated cells have significant difference with control cells (*$P < 0.05$, repeated-measures ANOVA).

membrane. Additional pipette aspiration studies that simultaneously monitor membrane capacitance and/or confirm changes in membrane folding by transmission electron microscopy could further probe the magnitude, origin, and functional significance of the OHC membrane reservoir.

The membrane reservoir is likely to be associated with nanoscale membrane curvature. Sal and CPZ are ionic amphipaths of opposite charge that alter PM curvature (Fig. 6). The theory of chemically induced bending moments (19) predicts that membrane bending results from an increase in the area of one leaflet relative to the other. The differential area expansion causes a bending in the direction of the layer into which the amphipath inserts. The tendency of an amphipath to intercalate in one layer or the other depends on its molecular shape and charge. Sal is expected to preferentially intercalate in a positively charged leaflet, whereas CPZ will prefer a negatively charged leaflet. In red blood cells, Sal causes outward membrane buckling (crenation) (34) whereas CPZ causes inward buckling (cupping) (58, 65, 66). The surface charge of the OHC membranes has not been directly measured, but negatively charged liposomes adhere to the OHC, suggesting that its outer membrane is positively charged (51).

Excess PM and OHC shape. The membrane contained in the ripples observed in electron microscopic studies (15) is likely to be the source of the vesicle membrane. During aspiration, it is likely that the rippling is lost, particularly as the vesicles form without the support of the CL (42). In contrast, during the volume increase resulting from the hypoosmotic fluid jet there is no change in apparent surface area (Fig. 3*D*), suggesting that the reduction in osmotic pressure resulting from water entry and an increased wall tension serve to maintain the apparent surface area of the

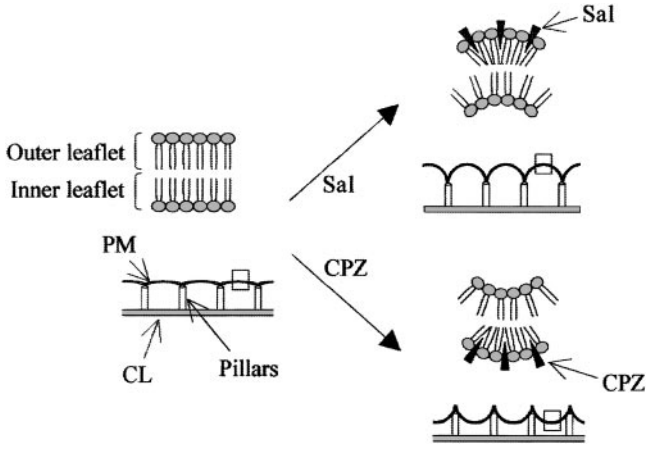

Fig. 6. Partition of ionic amphipaths in the PM. Sal intercalates into the positively charged outer leaflet of the PM and expands its area, causing the membrane to bend outward, whereas CPZ intercalates into the negatively charged inner leaflet, resulting in an inward bending of the membrane. CL, cortical lattice.

lateral wall constant in the face of increased cell volume. A membrane reservoir has implications for the mechanism of electromotility. Excess membrane area and the associated nanoscale rippling would decrease the efficiency of a mechanism based on area change or the development of in-plane strains. However, nanoscale rippling is consistent with the recently proposed membrane-bending motor model of electromotility (52). Moreover, the voltage- and tension dependence of lateral diffusion in the PM can be interpreted on the basis of nanoscale rippling (43).

Alteration of mechanical properties of PM. Figure 7 shows two steps of the vesiculation process. The first step occurs when the PM breaks away from the CL-SSC complex (Fig. 7*A*). The second step is when the PM stretches and elongates until a vesicle pinches off (Fig. 7*B*). As the PM stretches, it flows around the pillar attachment points. The nature of the PM's attachment to the pillars is unknown. Electron microscopic studies show that the pillars directly insert into the membrane (22). Integral membrane proteins are thought to prefer regions of the cell with a specific membrane curvature (12, 14, 33, 48). The connection between the pillars and the PM may require a PM with a local negative curvature (membrane bending into the cell). The drawings in Fig. 6 representing normal and Sal-treated cells show negative PM curvature at the point of pillar contact. If CPZ is acting on the nanoscale as it does on the microscale in red blood cells, then CPZ may reduce this negative curvature and possibly result in it becoming locally positive (as shown in Fig. 6). The change in curvature may contribute to the reduction in force that is required to form a vesicle. The dramatic decrease in the mean time for vesicle formation also supports the possibility that the pillar interacts primarily with the inner leaflet of the PM and that CPZ interferes with that interaction.

The second step of vesiculation must also involve consideration of the tension in the lateral wall. In APPENDIX B, we calculate the tension from the measured aspiration pressure (*Eq. B3*). This approach reveals that Sal and CPZ have opposing effects on the tension required to form a vesicle (see Fig. 4*B*). The differences between the drug treatments are consistent with other observations showing that crenators increase and cup formers (such as CPZ) decrease differential membrane tension (45). Theoretical models (39) and experimental observations (15, 16, 28) of membrane vesiculation resulting from ionic amphipaths predict a pivotal role for differential membrane tension. Drug-induced changes in membrane mechanics may play a role in effects of amphipaths on electromotility. Sal reduces OHC electromotility (15, 67), whereas CPZ has no effect on the magnitude of electromotility but shifts its operating voltage (38). In pure membranes, Sal disorders the lipid component of the bilayer (23) and reduces membrane mechanical strength (50). Sal also alters the deformability of the red blood cell (10). Both Sal and CPZ alter membrane fluidity in the OHC (43). CPZ and other amphipathic cup-forming agents decrease, whereas crenating agents increase, transmembrane currents in COS cells (45). The ability of Sal to alter membrane properties such as curvature, tension, and fluidity is in harmony with its ability to reversibly attenuate OHC electromotility and produce a reversible hearing loss. The ability of CPZ to shift the nonlinear capacitance may be due to a change in differential area elasticity (Ref. 49; Raphael RM, Popel AS, and Brownell WE, unpublished observation).

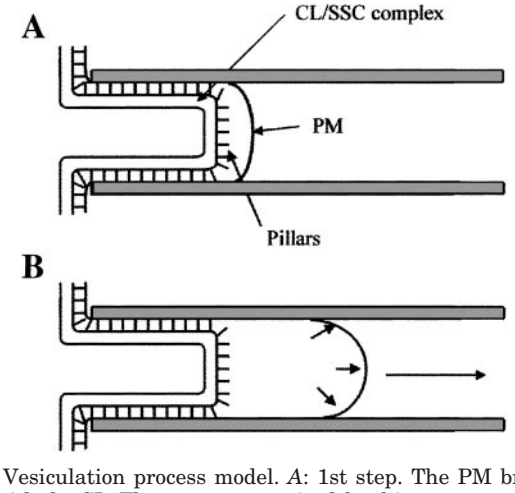

Fig. 7. Vesiculation process model. *A*: 1st step. The PM breaks its tether with the CL. The pressure required for this process most likely reflects the force of attachment between the PM and the pillars. *B*: 2nd step. Only the PM is stretched and elongating, with additional membrane flowing around the pillars into the growing "tongue"; eventually, the PM pinches off to form a vesicle.

Sal and CPZ decrease strain-dependent hydraulic conductivity. The OHC normally has low water permeability (11, 55, 56); however, there is an increase in water permeability when the PM is deformed (8). The observed loss of volume on aspiration and increase with the water jet are consistent with a strain-induced change in hydraulic conductivity. A possible mechanism for the increase in water permeability is the formation of small pores in the stretched membrane. Membranes naturally form defects that permit the movement of lipids between the leaflets and movement of nonpermeable solutes (54); the addition of mechanical tension could increase the probability of defect formation. We showed previously (8) that stretching the membrane leads to formation of pores that admit mono- and disaccharides but not raffinose, implying a pore size $\leq$4 nm. CPZ reduces the strain-induced increase in hydraulic conductivity. This may be related to its ability to decrease membrane tension (45) or antagonize the energy for pore formation, which depends on differential membrane tension. The minor change in radius of OHCs during aspiration of vesicles for control cells (Fig. 2*A*) reflects the loss of cytosol and associated reduction in cell turgor because of the strain-induced increase in hydraulic conductivity. The loss is reduced in the drug-treated cells.

Role of cytoskeleton in electromotility. Electromotility depends on the connection between the cytoskeleton and the PM. Our results indicate that CPZ loosens this connection when the cell is aspirated under high pressures. The fact that CPZ does not affect the magnitude

of electromotility implies that CPZ does not have a significant effect on the connectivity of the layers during normal electromotile generated strains. The intact OHC is predisposed to change length rather than diameter because the stiffness of the cytoskeleton is greater circumferentially than it is longitudinally (27). However, Sal- and CPZ-treated cells under aspiration change their shape (both length and radius), which suggests a contribution of the membranes to the elastic properties of the lateral wall (59). However, treatment with Sal and CPZ alone does not change the resting shape of OHCs. This implies that intercalation of these amphiphiles into the membrane does not generate enough force to overcome the cytoskeletal factors controlling cell shape. This also implies that although Sal and CPZ may affect the association of the PM and the CL, making them easier or harder to separate, these molecules do not affect the integrity of the cytoskeleton itself. Although it is possible that cytoskeletal remodeling occurs during the large deformations in the pipette that also contribute to the forces, the differential effect of Sal and CPZ are likely the result of effects on the membrane.

In conclusion, we have shown that amphipathic drugs change the mechanical properties of the OHC PM. Our results on the shape change during aspiration, the tension required for vesiculation, and the time to form a vesicle are rationalized in terms of differential tension. The existence of excess PM acting as a membrane reservoir coupled with changes in mechanical properties induced by amphipaths indicate that membrane curvature may be intricately linked to the molecular mechanism of electromotility.

APPENDIX A

Sources of Errors in Surface Area and Volume Measurements

In measuring cell surface area and volume, we incur both random errors (an individual measured value deviates from its expected value according to some probability distribution) and systematic errors (the expected value deviates from the true value). With this classification, four sources of measurement errors can be identified: *1*) random errors due to errors incurred in tracing the cell/vesicle outline; *2*) systematic errors caused by cell bending; *3*) systematic errors at the apical and basal ends of the cell; and *4*) systematic errors incurred if the cross section of the cell is not circular.

Error types 2–4 are all caused by discrepancies between the actual shape and the cylindrical shape of the segments assumed by the measurement algorithm. Given that vesicles are removed from the central portion of the cell, type 3 errors are likely to be the same before and after vesicle removal in a given cell. Type 3 errors are therefore unlikely to affect before/after comparisons and can be ignored for the purpose of this paper. The presence of type 4 errors has been addressed in a previous publication (11) where the cross-sectional profile was found to be circular by confocal microscopy. The strain-dependent increase in hydraulic conductivity leads to volume increases for both the aspiration and fluid jet experiments. Our morphometric analysis revealed a systematic increase in radius (Fig. 2*B*). Microscope focus was adjusted during the experiment to maintain the focal z-plane at the maximum cell diameter. If an increase in cell diameter were the result of the OHC flattening out, the focal plane would be closer to the glass substrate, which never occurred. The observed elevation in the focal plane was consistent with the OHC maintaining a circular profile.

Table 2. *Difference between measured and true values for a model cell*

	Bending Angle		
	0°	25°	30°
Radius	−2.098	−1.820	−1.503
Length	−1.180	−1.277	−0.760
Surface area	1.831	2.884	2.892
Volume	−0.854	2.252	4.411

Values are expressed in %.

Random (type 1) errors increase the number of observations necessary to establish a significant difference between two groups. Large random errors therefore limit our ability to resolve small differences but do not introduce spurious differences between groups. Systematic errors (type 2), on the other hand, have the potential to introduce such spurious differences into the results and must be considered carefully.

Random errors. With a Taylor series expansion, one can show that if the relative error (standard deviation ÷ expected value) of the measured radius r_i is α, the relative error in S_i and V_i will be α and 2α, respectively. However, because the total surface area and volume are computed as the sum of n cylindrical segments, the error in these parameters will be $\alpha/\sqrt{n}$ and $2\alpha/\sqrt{n}$, respectively. Thus, if $n = 100$, a 10% measurement error in radius will translate into 1% and 2% errors in total surface area and volume, respectively. Repeating the measurement five times and taking the average of the results further reduces the errors by a factor of $\sqrt{5}$.

A similar argument can be made for the surface area and volume of the cylindrical midportion of a vesicle. However, here, the length Δx is also a measured parameter with a measurement error, and the approximate errors will be 2α and 3α, respectively. Assuming that the midportion accounts for the majority of the vesicle area and volume, we can use this as a rough estimate of the relative error in these parameters. Thus, assuming a measurement error of 10% for the length and radius, the measurement error in vesicle area and volume may be as high as 20% and 30%, respectively. Again, repeating the measurement five times and taking the average of the results reduces the errors by a factor of $\sqrt{5}$ to ~9% and 13%, respectively. The impact of this error is further reduced by summing the vesicle surface area and volume in multiples of three vesicles and comparing the sum with either the initial surface and area of the cell or the total change (cell + Σvesicles) up to that point.

Systematic errors due to bending. From formulas for the surface area and volume of a circular torus (47), we can compute the surface area and volume of a segment.

$$S = \frac{\varphi}{2\pi} 4\pi^2 r_{t2} \frac{r_{t3} - r_{t1}}{2} = \varphi\pi r_{t2}(r_{t3} - r_{t1}) \qquad (A1)$$

and

$$V = \frac{\varphi}{2\pi} 2\pi^2 r_{t2} \left(\frac{r_{t3} - r_{t1}}{2}\right)^2 = \varphi\pi r_{t2} \left(\frac{r_{t3} - r_{t1}}{2}\right)^2 \qquad (A2)$$

where the angle describing a segment of torus is φ (this angle is zero if the cell is not bent), r_{t1} is the inner radius of the toroidal segment, r_{t2} is the radius to the center of the

toroidal segment, and r_{t3} is the outer radius. The surface area and volume of the cylindrical approximation in Fig. 1 are

$$S' = 2r_{t2} \sin\frac{\varphi}{2} \cdot \pi(r_{t3} - r_{t1}) = 2 \sin\frac{\varphi}{2} \cdot \pi r_{t2}(r_{t3} - r_{t1}) \quad (A3)$$

and

$$V' = 2r_{t2} \sin\frac{\varphi}{2} \cdot \pi\left(\frac{r_{t3} - r_{t1}}{2}\right)^2 = 2 \sin\frac{\varphi}{2} \cdot \pi r_{t2}\left(\frac{r_{t3} - r_{t1}}{2}\right)^2 \quad (A4)$$

The error incurred by using the approximations can thus be written as

$$1 - \frac{S}{S'} = 1 - \frac{V}{V'} = 1 - \frac{2 \sin\frac{\varphi}{2}}{\varphi} = 1 - \text{sinc}\frac{\varphi}{2} \quad (A5)$$

where $\text{sinc}(x) = \sin(x)/x$ and a positive error corresponds to an overestimation of the area or volume. Note that the value of the sinc function is one for a zero angle, i.e., the error in the estimate approaches zero as the angle φ approaches zero. If a "knee" in a cell with a large bending angle Φ is represented by n segments each having a bending angle $\varphi = \Phi/n$, the total error will be

$$e(\Phi, n) = n \cdot \left(1 - \text{sinc}\frac{\Phi}{2n}\right) \quad (A6)$$

For example, a 45° ($\pi/4$ radian) bend approximated by five segments would yield a total error of ~0.5%. This error is minor compared with the random errors, as can be appreciated by examination of Table 2, where measurements were made from a drawing representing the projection of a model cell and the calculated values compared with the true quantities represented by the model.

A determination of measurement was obtained by subjecting a model image of a cylindrical cell to the exact same analysis as the OHC images. Model images were generated having bending angles of 0° (straight) or buckled at 25° and 30°. The model images were traced 20 times with the MATLAB program, and the error was calculated (Table 2). In our experiments, some of the cells were bent up to 150°, but this was not correlated with drug application. The error for the model image was within 2% for length and radius and within 5% for surface area and volume. Therefore, the magnitude of possible errors does not alter the conclusions based on our measurements.

APPENDIX B

Theoretical Considerations for Calculation of Apparent Tension

To evaluate the effect of ionic amphipaths on cell mechanical properties, the aspiration pressure in the pipette must be related to the tension. We adopt the approach used for micropipette-aspirated red blood cells (18, 20). The lateral wall is treated as a continuum and is described mechanically by shell theory. Because the thickness of the lateral wall is 100 nm and the radius of the cell is 4 μm, the lateral wall can adequately be treated as a thin shell so long as it is realized that the calculated force resultants will be effective parameters that are distributed between the membrane and the cytoskeleton. Assuming that the transverse shear component does not vary with position on the surface, in-plane force resultants (tensions) can simply be related to hydrostatic pressure differences scaled by the radius of curvature (the classic law of Laplace) (17, 20). In the analysis of the micropipette experiment, assuming tension in the pipette (τ_p) is isotropic, force balance in the pipette predicts that

$$\tau_p = \frac{R_p(P_p - P_i)}{2} \quad (B1)$$

where P_p equals aspiration pressure in the pipette (in mN/m^2), P_i equals the pressure inside the cell, and R_p equals inner radius of the micropipette (in μm). The pressure inside the cell is an unknown. To eliminate it, we apply the law of Laplace to the portion of the cell outside the micropipette. The outer portion of the cell is anisotropic: the membrane tension in the longitudinal direction is

$$\tau_l = \frac{R_c(P_i - P_o)}{2} \quad (B2)$$

where P_o is the external pressure and R_c equals the average radius of the cell.

Equating τ_p and τ_l and combining *Eqs. B1* and *B2* gives an equation for estimating the tension in the lateral wall

$$\tau_l = \frac{\Delta P R_c R_p}{2(R_c + R_p)} \quad (B3)$$

where $\Delta P = P_p - P_o$.

This tension must be viewed as an "apparent" tension and must not be interpreted as the tension residing in the plasma membrane. The OHC has a complex trilamellar lateral wall and is best modeled as an orthotropic cylindrical shell (72), meaning that there may be a contribution from the circumferential tension. In applying *Eq. B3*, we have assumed that this apparent tension "turns the corner" of the pipette and remains the same in the far field. In reality, there is likely to be a tension gradient as the membrane leaves the pipette that would affect the absolute magnitude of the calculated tension. However, we only claim the validity of this analysis up to the point at which the vesicle separates from the membrane. After this event, the mechanical analysis becomes more complicated. Nevertheless, our approach provides a framework for the interpretation of experiments on drug effects (see Fig. 4*B*).

We thank A. S. Popel and J. S. Oghalai for helpful comments.

This work supported by National Institute of Deafness and Other Communications Disorders Grants DC-00354, DC-02775, and National Research Service Award DC-00363 and National Science Foundation Grant 9871994.

Present addresses: N. Morimoto, Dept. of Otolaryngology, National Children's Hospital, 3-35-31 Taishido Setagaya, Tokyo 154-8509, Japan (E-mail: nmorimoto@nch.go.jp); R. M. Raphael, Department of Bioengineering, MS142, Rice University, Houston, TX 77251-1892 (E-mail: rraphael@rice.edu); A. Nygren, Dept of Physiology and Biophysics, University of Calgary, 3300 Hospital Dr NW, Calgary, AB, Canada T2N 4N1 (E-mail: nygren@ucalgary.ca).

REFERENCES

1. **Anvari B, Li Z, Takashima M, Brecht P, Torres JH, and Brownell WE.** Dynamic tether force measurements of the outer hair cell plasma membrane with optical tweezers. *SPIE Proc* 4260: 103–108, 2001.
2. **Arima T, Kuraoka A, Toriya R, Shibata Y, and Uemura T.** Quick-freeze, deep-etch visualization of the "cytoskeletal spring" of cochlear outer hair cells. *Cell Tissue Res* 263: 91–97, 1991.
3. **Bannister LH, Dodson HC, Astbury AR, and Douek EE.** The cortical lattice: a highly ordered system of subsurface filaments in guinea pig cochlear outer hair cells. *Prog Brain Res* 74: 213–219, 1988.

4. **Bloom M, Evans E, and Mouritsen OG.** Physical properties of the fluid lipid-bilayer component of cell membranes: a perspective. *Q Rev Biophys* 24: 293–397, 1991.
5. **Brownell WE.** Outer hair cell electromotility and otoacoustic emissions. *Ear Hear* 11: 82–92, 1990.
6. **Brownell WE, Bader CR, Bertrand D, and de Ribaupierre Y.** Evoked mechanical responses of isolated cochlear outer hair cells. *Science* 227: 194–196, 1985.
7. **Brownell WE and Kachar B.** Outer hair cell motility: a possible electro-kinetic mechanism. In: *Peripheral Auditory Mechanisms*, edited by Allen JB, Hall JL, Hubbard AE, Neely ST, and Tubis A. Berlin: Springer, 1986, p. 369–376.
8. **Brownell WE, Ratnanather JT, Popel AS, Zhi M, and Sit PS.** Labyrinthine lateral walls: cochlear outer hair cell permeability and mechanics. In: *Active Hearing*, edited by Flock A, Ottoson D, and Ulfendahl M. Amsterdam: Elsevier Science, 1995, p. 167–179.
9. **Brownell WE, Spector AA, Raphael RM, and Popel AS.** Micro- and nanomechanics of the cochlear outer hair cell. Annu Rev Biomed Eng 3: 169–194, 2001.
10. **Chabanel A, Reinhart W, and Chien S.** Increased resistance to membrane deformation of shape-transformed human red blood cells. *Blood* 69: 739–743, 1987.
11. **Chertoff ME and Brownell WE.** Characterization of cochlear outer hair cell turgor. *Am J Physiol Cell Physiol* 266: C467–C479, 1994.
12. **Chou T, Jaric MV, and Siggia ED.** Electrostatics of lipid bilayer bending. *Biophys J* 72: 2042–2055, 1997.
13. **Dallos P, Evans BN, and Hallworth R.** Nature of the motor element in electrokinetic shape changes of cochlear outer hair cells. *Nature* 350: 155–157, 1991.
14. **Dan N and Safran SA.** Effect of lipid characteristics on the structure of transmembrane proteins. *Biophys J* 75: 1410–1414, 1998.
15. **Dieler R, Shehata-Dieler WE, and Brownell WE.** Concomitant salicylate-induced alterations of outer hair cell subsurface cisternae and electromotility. *J Neurocytol* 20: 637–653, 1991.
16. **Dieler R, Shehata-Dieler WE, Richter CP, and Klinke R.** Effects of endolymphatic and perilymphatic application of salicylate in the pigeon. II. Fine structure of auditory hair cells. *Hear Res* 74: 85–98, 1994.
17. **Evans E and Yeung A.** Hidden dynamics in rapid changes of bilayer shape. *Chem Phys Lipids* 73: 39–56, 1994.
18. **Evans EA.** New membrane concept applied to the analysis of fluid shear- and micropipette-deformed red blood cells. *Biophys J* 13: 941–954, 1973.
19. **Evans EA.** Bending resistance and chemically induced moments in membrane bilayers. *Biophys J* 14: 923–931, 1974.
20. **Evans EA and Skalak R.** *Mechanics and Thermodynamics of Biomembranes*. Boca Raton, FL: CRC, 1980.
21. **Flock A, Flock B, and Ulfendahl M.** Mechanisms of movement in outer hair cells and a possible structural basis. *Arch Otorhinolaryngol* 243: 83–90, 1986.
22. **Forge A.** Structural features of the lateral walls in mammalian cochlear outer hair cells. *Cell Tissue Res* 265: 473–483, 1991.
23. **Ghosh AK, Basu R, Dey S, Das S, Nayak NP, Barat B, and Nandy P.** Lipid-disordering effect of aspirin on the liposomal membrane of dipalmitoyl phosphatidyl choline—a fluorescence anisotropy study. *Colloids Surfaces B* 4: 309–311, 1995.
24. **Hallworth R.** Modulation of outer hair cell compliance and force by agents that affect hearing. *Hear Res* 114: 204–212, 1997.
25. **Holley MC and Ashmore JF.** A cytoskeletal spring in cochlear outer hair cells. *Nature* 335: 635–637, 1988.
26. **Holley MC and Ashmore JF.** Spectrin, actin and the structure of the cortical lattice in mammalian cochlear outer hair cells. *J Cell Sci* 96: 283–291, 1990.
27. **Holley MC, Kalinec F, and Kachar B.** Structure of the cortical cytoskeleton in mammalian outer hair cells. *J Cell Sci* 102: 569–580, 1992.
28. **Hueck IS, Hollweg HG, Schmid-Schönbein GW, and Artmann GM.** Chlorpromazine modulates the morphological macro- and microstructure of endothelial cells. *Am J Physiol Cell Physiol* 278: C873–C878, 2000.
29. **Iwasa KH.** A membrane motor model for the fast motility of the outer hair cell. *J Acoust Soc Am* 96: 2216–2224, 1994.
30. **Kachar B, Brownell WE, Altschuler RA, and Fex J.** Electrokinetic shape changes of cochlear outer hair cells. *Nature* 322: 365–368, 1986.
31. **Kakehata S and Santos-Sacchi J.** Membrane tension directly shifts voltage dependence of outer hair cell motility and associated gating charge. *Biophys J* 68: 2190–2197, 1995.
32. **Kakehata S and Santos-Sacchi J.** Effects of salicylate and lanthanides on outer hair cell motility and associated gating charge. *J Neurosci* 16: 4881–4889, 1996.
33. **Kim KS, Neu J, and Oster G.** Curvature-mediated interactions between membrane proteins. *Biophys J* 75: 2274–2291, 1998.
34. **Li A, Seipelt H, Muller C, Shi Y, and Artmann M.** Effects of salicylic acid derivatives on red blood cell membranes. *Pharmacol Toxicol* 85: 206–211, 1999.
35. **Li Z, Anvari B, Takashima M, Brecht P, Torres JH, and Brownell WE.** Membrane tether formation from outer hair cells with optical tweezers. *Biophys J* 82: 1386–1395, 2002.
36. **Ludwig J, Oliver D, Frank G, Klocker N, Gummer AW, and Fakler B.** Reciprocal electromechanical properties of rat prestin: The motor molecule from rat outer hair cells. *Proc Natl Acad Sci USA* 98: 4178–4183, 2001.
37. **Lue AJ and Brownell WE.** Salicylate induced changes in outer hair cell lateral wall stiffness. *Hear Res* 135: 163–168, 1999.
38. **Lue AJ, Zhao HB, and Brownell WE.** Chlorpromazine alters outer hair cell electromotility. *Otolaryngol Head Neck Surg* 125: 71–76, 2001.
39. **Miao L, Seifert U, Wortis M, and Dobereiner HG.** Budding transitions of fluid-bilayer vesicles: the effect of area-difference elasticity. *Phys Rev E* 49: 5389–5407, 1994.
40. **Morimoto N, Nygren A, and Brownell WE.** Quantitative assessment of drug-induced change in OHC lateral wall mechanics. In: *Recent Developments in Auditory Mechanics*, edited by Wada H, Takasaka T, Ikeda K, Ohyama K and Koike T. Singapore: World Scientific, 2000, p. 261–267.
41. **Needham D and Zhelev DV.** Lysolipid exchange with lipid vesicle membranes. *Ann Biomed Eng* 23: 287–298, 1995.
42. **Oghalai JS, Patel AA, Nakagawa T, and Brownell WE.** Fluorescence-imaged microdeformation of the outer hair cell lateral wall. *J Neurosci* 18: 48–58, 1998.
43. **Oghalai JS, Zhao HB, Kutz JW, and Brownell WE.** Voltage- and tension-dependent lipid mobility in the outer hair cell plasma membrane. *Science* 287: 658–661, 2000.
44. **Oliver D, He DZ, Klocker N, Ludwig J, Schulte U, Waldegger S, Ruppersberg JP, Dallos P, and Fakler B.** Intracellular anions as the voltage sensor of prestin, the outer hair cell motor protein. *Science* 292: 2340–2343, 2001.
45. **Patel AJ, Honore E, Maingret F, Lesage F, Fink M, Duprat F, and Lazdunski M.** A mammalian two pore domain mechanogated S-like K^+ channel. *EMBO J* 17: 4283–4290, 1998.
46. **Pollice PA and Brownell WE.** Characterization of the outer hair cell's lateral wall membranes. *Hear Res* 70: 187–196, 1993.
47. **Råde L and Westergren B.** *BETA: Mathematics Handbook*. Lund, Sweden: Studentlitteratur, 1990.
48. **Ramaswamy S, Toner J, and Prost J.** Nonequilibrium fluctuations, traveling waves, and instabilities in active membranes. *Phys Rev Lett* 84: 3494–3497, 2000.
49. **Raphael RM.** A membrane bending mechanism for nanoelectromechanical transduction in cochlear outer hair cells. *Proc 2001 Summer Bioeng Res Conf* 50: 867–868, 2001.
50. **Raphael RM, Nguyen TA, and Popel AS.** Salicylate induced softening of membrane bilayers. *Biophys J* 76: A273, 1999.
51. **Raphael RM and Popel AS.** Adhesion of liposomal membranes to outer hair cells requires negatively charged and nonbilayer lipids: implications for liposomal vector design. *Association for Research in Otolaryngology Abstracts*, edited by Santi PA. St. Petersburg Beach, FL: Association for Research in Otolaryngology, 2001, p. 72.
52. **Raphael RM, Popel AS, and Brownell WE.** A membrane bending model of outer hair cell electromotility. *Biophys J* 78: 2844–2862, 2000.

54. **Raphael RM, Waugh RE, Svetina S, and Zeks B.** Fractional occurrence of defects in membranes and mechanically driven interleaflet phospholipid transport. *Phys Rev E* 64: 1913–1922, 2001.
55. **Ratnanather JT, Popel AS, and Brownell WE.** An analysis of the hydraulic conductivity of the extracisternal space of the cochlear outer hair cell. *J Math Biol* 40: 372–382, 2000.
56. **Ratnanather JT, Zhi M, Brownell WE, and Popel AS.** Measurements and a model of the outer hair cell hydraulic conductivity. *Hear Res* 96: 33–40, 1996.
57. **Raucher D and Sheetz MP.** Characteristics of a membrane reservoir buffering membrane tension. *Biophys J* 77: 1992–2002, 1999.
58. **Rosso J, Zachowski A, and Devaux PF.** Influence of chlorpromazine on the transverse mobility of phospholipids in the human erythrocyte membrane: relation to shape changes. *Biochim Biophys Acta* 942: 271–279, 1988.
59. **Russell IJ and Schauz C.** Salicylate ototoxicity: effects of the stiffness and electromotiliy of outer hair cells isolated from the guinea pig cochlea. *Aud Neurosci* 1: 309–320, 1995.
60. **Saito K.** Fine structure of the sensory epithelium of guinea-pig organ of Corti: subsurface cisternae and lamellar bodies in the outer hair cells. *Cell Tissue Res* 229: 467–481, 1983.
61. **Santos-Sacchi J.** Reversible inhibition of voltage-dependent outer hair cell motility and capacitance. *J Neurosci* 11: 3096–3110, 1991.
62. **Santos-Sacchi J.** Harmonics of outer hair cell motility. *Biophys J* 65: 2217–2227, 1993.
63. **Santos-Sacchi J, Shen W, Zheng J, and Dallos P.** Effects of membrane potential and tension on prestin, the outer hair cell lateral membrane motor protein. *J Physiol (Lond)* 531: 661–666, 2001.
64. **Schmid-Schönbein GW, Kosawada T, Skalak R, and Chien S.** Membrane model of endothelial cells and leukocytes. A proposal for the origin of a cortical stress. *J Biomech Eng* 117: 171–178, 1995.
65. **Schrier SL, Zachowski A, and Devaux PF.** Mechanisms of amphipath-induced stomatocytosis in human erythrocytes. *Blood* 79: 782–786, 1992.
66. **Sheetz MP and Singer SJ.** Biological membranes as bilayer couples. A molecular mechanism of drug- erythrocyte interactions. *Proc Natl Acad Sci USA* 71: 4457–4461, 1974.
67. **Shehata WE, Brownell WE, and Dieler R.** Effects of salicylate on shape, electromotility and membrane characteristics of isolated outer hair cells from guinea pig cochlea. *Acta Otolaryngol (Stockh)* 111: 707–718, 1991.
68. **Siegel JH and Brownell WE.** Synaptic and golgi membrane recycling in cochlear hair cells. *J Neurocytol* 15: 311–328, 1986.
69. **Sit PS, Spector AA, Lue AJ, Popel AS, and Brownell WE.** Micropipette aspiration on the outer hair cell lateral wall. *Biophys J* 72: 2812–2819, 1997.
70. **Smith CA.** Ultrastructure of the organ of Corti. *Adv Sci* 122: 419–433, 1968.
71. **Spector AA, Ameen M, Charalambides PG, and Popel AS.** Computational modeling of the outer hair cell cytoskeleton. In: *Recent Developments in Auditory Mechanics*, edited by Wada H, Takasaka T, Ikeda K, Ohyama K, and Koike T. Singapore: World Scientific, 2000, p. 307–313.
72. **Spector AA, Brownell WE, and Popel AS.** Mechanical and electromotile characteristics of auditory outer hair cells. *Med Biol Eng Comput* 37: 247–251, 1999.
73. **Spector AA, Brownell WE, and Popel AS.** Nonlinear active force generation by cochlear outer hair cell. *J Acoust Soc Am* 105: 2414–2420, 1999.
74. **Tunstall MJ, Gale JE, and Ashmore JF.** Action of salicylate on membrane capacitance of outer hair cells from the guinea-pig cochlea. *J Physiol (Lond)* 485: 739–752, 1995.
75. **Ulfendahl M and Slepecky N.** Ultrastructural correlates of inner ear sensory cell shortening. *J Submicrosc Cytol Pathol* 20: 47–51, 1988.
76. **Vlahakis NE and Hubmayr RD.** Invited review: plasma membrane stress failure in alveolar epithelial cells. *J Appl Physiol* 89: 2490–2497, 2000.
77. **Wu M and Santos-Sacchi J.** Effects of lipophilic ions on outer hair cell membrane capacitance and motility. *J Membr Biol* 166: 111–118, 1998.
78. **Zheng J, Shen W, He DZ, Long KB, Madison LD, and Dallos P.** Prestin is the motor protein of cochlear outer hair cells. *Nature* 405: 149–155, 2000.